Geophysical Research Letters

RESEARCH LETTER
10.1029/2020GL087132

Trends in AOD, Clouds, and Cloud Radiative Effects in Satellite Data and CMIP5 and CMIP6 Model Simulations Over Aerosol Source Regions

Ribu Cherian[1] **and Johannes Quaas**[1]

[1]Institute for Meteorology, Universität Leipzig, Leipzig, Germany

Key Points:
- Strong trends in AOD in aerosol source regions during 2001 to 2017 reflected in cloud droplet number concentration trends
- The CMIP6 multimodel ensemble shows improved results compared to CMIP5 pointing to improved anthropogenic aerosol emissions
- Model results in LWP inconsistent with data: trends in CRE match observations due to compensating errors in cloud fraction trends

Supporting Information:
- Supporting Information S1

Correspondence to:
R. Cherian,
ribu.cherian@uni-leipzig.de

Citation:
Cherian, R., & J. Quaas (2020). Trends in AOD, clouds, and cloud radiative effects in satellite data and CMIP5 and CMIP6 model simulations over aerosol source regions. *Geophysical Research Letters*, *47*, e2020GL087132. https://doi.org/10.1029/2020GL087132

Received 17 JAN 2020
Accepted 6 APR 2020
Accepted article online 17 APR 2020

Abstract Several regions worldwide have seen significant trends in anthropogenic aerosol emissions during the period of detailed satellite observations since 2001. Over Europe (EUR) and North America (NAM) there were strong declines, over China increases then declines and over India, strong increases. Regional trends in model-simulated aerosol optical depth (AOD) and cloud radiative effects in both the Fifth and Sixth Coupled Model Intercomparison Projects (CMIP5 and CMIP6) are broadly consistent with the ones from satellite retrievals in most parts of EUR, NAM and India. CMIP6 models better match satellite-derived AOD trend in western NAM (increasing) and eastern China (decreasing), where CMIP5 models failed, pointing to improved anthropogenic aerosol emissions. Drop concentration trends in both observations and models qualitatively match AOD trends. The result for solar cloud radiative effect in models, however, is due to compensating errors: Models fail to reproduce observed liquid water path trends and show, in turn, opposite trends in cloud fraction.

Plain Language Summary Historically, widespread changes in regional air pollution have occurred, with emission reductions over the United States and Europe in response to air quality controls since the mid-1980s, and a general increase over Asia since the 1970s. In this study we found that current climate models with improved emission estimates match the regional aerosol and cloud trends derived from satellite observations over United States, Europe, China, and India regions. Further analysis revealed that good representation of regional solar cloud radiative effect trend is due to compensating errors in cloud trend in the models.

1. Introduction

In recent decades, anthropogenic aerosol emissions have decreased substantially because of air pollution reduction policies implemented in several regions and have increased substantially in others in which in particular fossil fuel consumption increased strongly (Smith & Bond, 2014; Stohl et al., 2015). Specifically, large changes of aerosol concentrations occurred over Europe (EUR) and North America (NAM) between 1950 and 1970 driven by strong increase in anthropogenic emissions and by emission reductions since the mid-1980s in response to air quality measures, and a general increase occurred over Asia and Africa since the 1970s (Klimont et al., 2013; Smith & Bond, 2014). This increase in the 21st century was particularly strong and steady over India. Aerosols interact with radiation (formerly known as "aerosol direct effect") and with clouds ("aerosol indirect effect"), so that the anthropogenic aerosol emission results in the effective radiative forcing (ERF) due to aerosol-cloud interactions (Bellouin et al., 2019). Consequently, a change in regional aerosol emissions is expected to affect the radiation budget and cloud properties. As an example, trends in cloud properties over China have been linked to changes in aerosol concentrations (Benas et al., 2020; Bennartz et al., 2011; Qian, Gong, et al., 2009). Similarly, changes in cloud properties were found in satellite data over EUR (Krüger & Graßl, 2002). Observed decadal trends in surface solar radiation over EUR and NAM have been linked to changes in aerosol emissions since the mid-1980s (Wild et al., 2005). Current aerosol-climate models successfully simulate the trends in aerosols (Aas et al., 2019) and suggest corresponding changes in radiative forcing over the last decades (Myhre et al., 2017).

Satellite derived and surface based aerosol optical depth (AOD) shows a positive trend over Southeast Asia while regions of EUR and United States exhibit negative trends (Wei, Peng, Mahmood, et al., 2019; Yu et al., 2020) and negative AOD trends over oceans (Jongeward et al., 2016; Yu et al., 2020). Satellite observed liquid

water path (LWP) shows a slight negative trend globally and significant regional variations (e.g.,decreases over North Atlantic and southeast Indian Ocean and increases over northwest Indian Ocean) Manaster et al., 2017 and Norris et al., 2016. Satellite derived cloud cover and cloud amount have undergone significant regional variations (e.g., cloudiness has increased in northwest Indian Ocean, and to the north Pacific and Atlantic oceans) in recent decades (1980s to 2000) (Geiss & Marchand, 2019; Norris et al., 2016). Loeb et al. (2007) found that cloud radiative effect (CRE) decadal trends also exhibit regional variations with greater variability in the tropics. However, the link between the trend in clouds and aerosols and their influence on the CRE trend is not well understood.

Aerosol-cloud interactions are a potentially relevant influence on cloud properties, and constitute the largest uncertainty in climate change forcing (Boucher et al., 2013; Myhre et al., 2013). The radiative forcing due to aerosol-cloud interactions is a consequence of the enhanced cloud droplet number concentration (CDNC) at larger aerosol concentrations (Gryspeerdt et al., 2016; Hasekamp et al., 2019; Twomey, 1974). The change in CDNC leads to rapid cloud adjustments, especially changes in cloud horizontal extent (cloud fraction, CF) and LWP. Several mechanisms are discussed for these adjustments, such as reductions in the autoconversion sink (Albrecht, 1989) and in the mixing-evaporation sink (Ackerman et al., 2004). Global satellite observations demonstrate that CF tends to increase at larger aerosol concentrations (Gryspeerdt et al., 2016) and that the LWP response is a balance between increases and decreases (Gryspeerdt et al., 2019), with an overall slight decrease (Toll et al., 2019).

Although significant improvements have been made to the Coupled Model Intercomparison Project Phase 5 (CMIP5) models (Boucher et al., 2013; Dolinar et al., 2015; Flato et al., 2013; Jiang et al., 2012; Klein et al., 2013; Lauer & Hamilton, 2013; Stanfield et al., 2014; 2015; Wang & Su, 2013), clouds and their radiative feedbacks are still a problem in climate models (Flato et al., 2013). Lauer and Hamilton (2013) have revealed that the CMIP5 model-simulated CREs tend to outperform CFs, suggesting that models are not accurately depicting fundamental cloud processes. It is also found that the CMIP5 multimodel ensemble mean CF, on average, is too low by 7% when compared to satellite observations, but there are good agreements in the simulated top-of-atmosphere radiation budget (Dolinar et al., 2015). In general, CMIP5 simulated AOD, CF, and CREs, agree with observations within a certain range on a global scale, but not on regional scale (Dolinar et al., 2015; Fan et al., 2018; Stanfield et al., 2014). GCMs to date are also inconsistent with the slight LWP decrease that satellite statistics suggest (Malavelle et al., 2017; Michibata et al., 2016; Toll et al., 2017).

Despite this, climate models with more comprehensive aerosol-cloud interactions simulate regional surface temperature trends better than other models (Ekman, 2014) and also are better in simulating meridional shifts in the general circulation (Chung & Soden, 2017). Recently, new results have become available from CMIP6 as well (Eyring et al., 2016). It is thus very interesting to assess to what extent the newer-generation models possibly show improved characteristics.

This study builds on past analyses that showed how the trend in EUR aerosol emissions and, in consequence, of the surface solar radiation may be used as an "emergent constraint" (Klein & Hall, 2015) for the aerosol ERF (Cherian et al., 2014). Such studies so far have not allowed one to assess the mechanisms of aerosol ERF (Norris & Wild, 2007).

The focus of this study is to understand the influence of aerosol emission trends on clouds and short-wave (solar, SW CRE) over regions with distinct long-term trends in anthropogenic aerosol emissions. Section 2 describes the CMIP5 and CMIP6 models and the satellite data used for the present study. The aerosol emission regional trend analysis and results from the comparison of the CMIP5 and CMIP6 models with satellite observations are presented in section 3. The main conclusions are given in section 4.

2. Methodology

In order to understand the link between aerosol emission trends and CREs, the CMIP5 and CMIP6 model-simulated SO_2 emissions, AOD at 550 nm, CDNC, LWP, CF, and SW and long-wave (LW) CREs ($R_{cld,sw}$ and $R_{cld,lw}$) are analyzed. The analysis is carried out for the period from 2001 to 2017 by using the multimodel simulations from CMIP5 "historical," "historical GHG," and "RCP4.5" experiment data sets (Taylor et al., 2012) and from CMIP6 "historical" and "ssp245" experiment data sets (Eyring et al., 2016; O'Neill et al., 2016). All the models that used interactive aerosol schemes and performed all the relevant experiments are considered for the present analysis. The CMIP5 and CMIP6 models used in the present study are given in

Geophysical Research Letters

10.1029/2020GL087132

Table 1
List of the Models Contributing to the CMIP5 and CMIP6 Experiments That Are Used in This Study, the Centers Leading the Modeling Efforts, the Model Resolutions, and Number of Ensemble Members

Lab/Institute	Institute ID/ country	Model name	Resolution	No. of ensemble members	References
(a) CMIP5					
Canadian Centre for Climate Modelling and Analysis	CCCMA/ Canada	CanESM2	128 × 64, L35	5	Arora et al. (2011)
Geophysical Fluid Dynamics Laboratory	NOAA GFDL/ USA	GFDL-CM3	144 × 90, L48	1	Donner et al. (2011)
Goddard Institute for Space Studies, NASA	NASA-GISS/ USA	GISS-E2-R GISS-E2-H	144 × 90, L40	5	Kim et al. (2012)
Institut Pierre Simon Laplace	IPSL/ France	IPSL-CM5A-LR	96 × 96, L39	3	Dufresne et al. (2013)
Met Office Hadley Centre for Climate	MOHC/ UK	HadGEM2-ES	192 × 145, L38	4	Jones et al. (2011)
Model for Interdisciplinary Research On Climate/ Atmos. Ocean Res. Ins., U. Tokyo/ Japan Agency for Marine-Earth Sci. & Tech., Japan	MIROC/ Japan	MIROC5	256 × 128, L40	3	Watanabe et al. (2010)
Norwegian Climate Centre	NCC / Norway	NorESM1-M	144 × 96, L26	1	Bentsen et al. (2013)
(b) CMIP6					
Canadian Centre for Climate Modelling and Analysis	CCCMA/ Canada	CanESM5	128 × 64, L49	3	Swart et al. (2019)
Geophysical Fluid Dynamics Laboratory	NOAA GFDL/ USA	GFDL-CM4	360 × 180, L33	1	Held et al. (2019)
Institut Pierre Simon Laplace	IPSL/ France	IPSL-CM6A-LR	144 × 143, 79	3	Boucher et al. (2018)
Met Office Hadley Centre for Climate	MOHC/ UK	HadGEM3-GC31-LL	192 × 144, L85	3	Roberts (2017)
Model for Interdisciplinary Research On Climate/ Atmos. Ocean Res. Ins., U. Tokyo/ Japan Agency for Marine-Earth Sci. & Tech., Japan	MIROC/ Japan	MIROC-ES2L	128 × 64, L40	3	Hajima et al. (2019)

Table 1. Multimodel diversity in statistical trends of aerosols and clouds are examined. In order to separate different regimes of aerosol emission trends, the analysis is carried out separately for four major anthropogenic source regions: EUR, NAM, China, and India (Figure S1 in the supporting information). For China, the trend analysis is split into two time periods: first the period of increasing emissions (from 2001 to 2005) and then of decreasing emissions (from 2006 to 2017), based on CMIP6 emissions (Figure S2).

CRE is the difference between the net top-of-atmosphere radiation fluxes, downwelling minus upwelling, of all-sky conditions minus clear-sky conditions (Dong & Mace, 2003; Ramanathan, 1989; Stanfield et al., 2015). The model-simulated LWP values are obtained by subtracting the vertically integrated ice water path from the vertically integrated cloud water path (ice + liquid). (IPSL-CM5A model provided only the vertically integrated LWP as cloud liquid water vertically integrated (https://pcmdi.llnl.gov/mips/cmip5/errata.html), and thus, we treat cloud liquid water vertically integrated from this model as liquid water only in the analysis.) To match the satellite definition, in-cloud LWP is computed by dividing the model-diagnosed all-sky LWP by the CF.

Cloud and aerosol retrievals from the Moderate Resolution Imaging Spectroradiometer (MODIS) instruments onboard the Terra satellite are used in this work (Levy et al., 2013; Platnick et al., 2017). The MODIS CDNC burden (m^{-2}) is derived using satellite-retrieved cloud optical depth and cloud effective radius by followingQuaas et al. (2006). The MODIS LWP ($g\,m^{-2}$) is used from MOD08 Level-3 data for liquid single layer clouds; the same product also provides AOD at 550 nm and CF. CRE ($W\,m^{-2}$) data are from the Clouds And The Earth's Radiant Energy System instrument on Terra. The time period considered is 2001–2017, and the data are used at monthly resolution. For each model the "historical" and "RCP4.5" experiments (CMIP5; "historical" until 2005) and "historical" and "ssp245" experiments (CMIP6; "historical" until 2014) were combined to create a time series that spanned the exact same length as the satellite observations.

3. Results and Discussion

3.1. Comparison of Simulated and Satellite-Derived Trends

The multimodel-simulated linear trends for AOD, vertically integrated CDNC (m^{-2}), LWP (gm^{-2}), CF, and SW and LW CRE (Wm^{-2}) from CMIP5 and CMIP6 trends are compared against satellite-derived ones for the EUR, NAM, India, and China regions separately.

3.1.1. Aerosol Optical Depth

Figure 1 shows the CMIP5 and CMIP6 model-simulated EUR trends compared to the satellite-derived trends. As expected, AOD in both models and satellite data show decreasing trends over EUR during this period. Both CMIP5 and CMIP6 models match the AOD trends over much of the continent. There is, however, a discrepancy between model and satellite trends in north-western parts of EUR.

For NAM, AOD in both model ensembles (CMIP5 and CMIP6) and satellite data show decreasing trends over eastern NAM (Figures 2a–2d). The observed increasing AOD trend over western NAM is of much smaller spatial extent in the CMIP6 models, but of similar magnitude, and of too little extent and too small magnitude in the CMIP5 models. The improvement in CMIP6 compared to CMIP5 is due to updated anthropogenic aerosol emission inventories used in CMIP6 models (Figure S2). The discrepancy over NAM is apparent in many of the individual model runs as well. Previous studies suggested that low rainfall and resultant enhanced fire activity which occurred over parts of the western NAM may lead to the positive trends in MODIS AOD (Yoon et al., 2014). Also, a recent study revealed that MODIS aerosol products failed to capture the correct temporal aerosol variations over western NAM, with only few sites showing the same signs between the MODIS and aeronet AOD trends (Wei, Peng, Guo, et al., 2019). Increases in BC and OC emissions, not SO_2, lead to the positive western NAM AOD trends in CMIP6 models (Figure S5). BC and OC steadily grow in NAM due to increases in residential biomass emissions (Gidden et al., 2019; Hoesly et al., 2018). In general, large regional variability in observed low AOD values (0.1–0.2) along with uncertainties in the emission inventories (wildfire activities) may explain the difference between the AOD trend over the western NAM region.

For India, both model ensembles and satellite data show an increasing trend during this period (Figures 3a–3d). Both CMIP5 and CMIP6 models capture the spatial extent and sign of the observed AOD trends. The magnitude is underestimated in CMIP5 models and matches better the satellite retrievals in CMIP6.

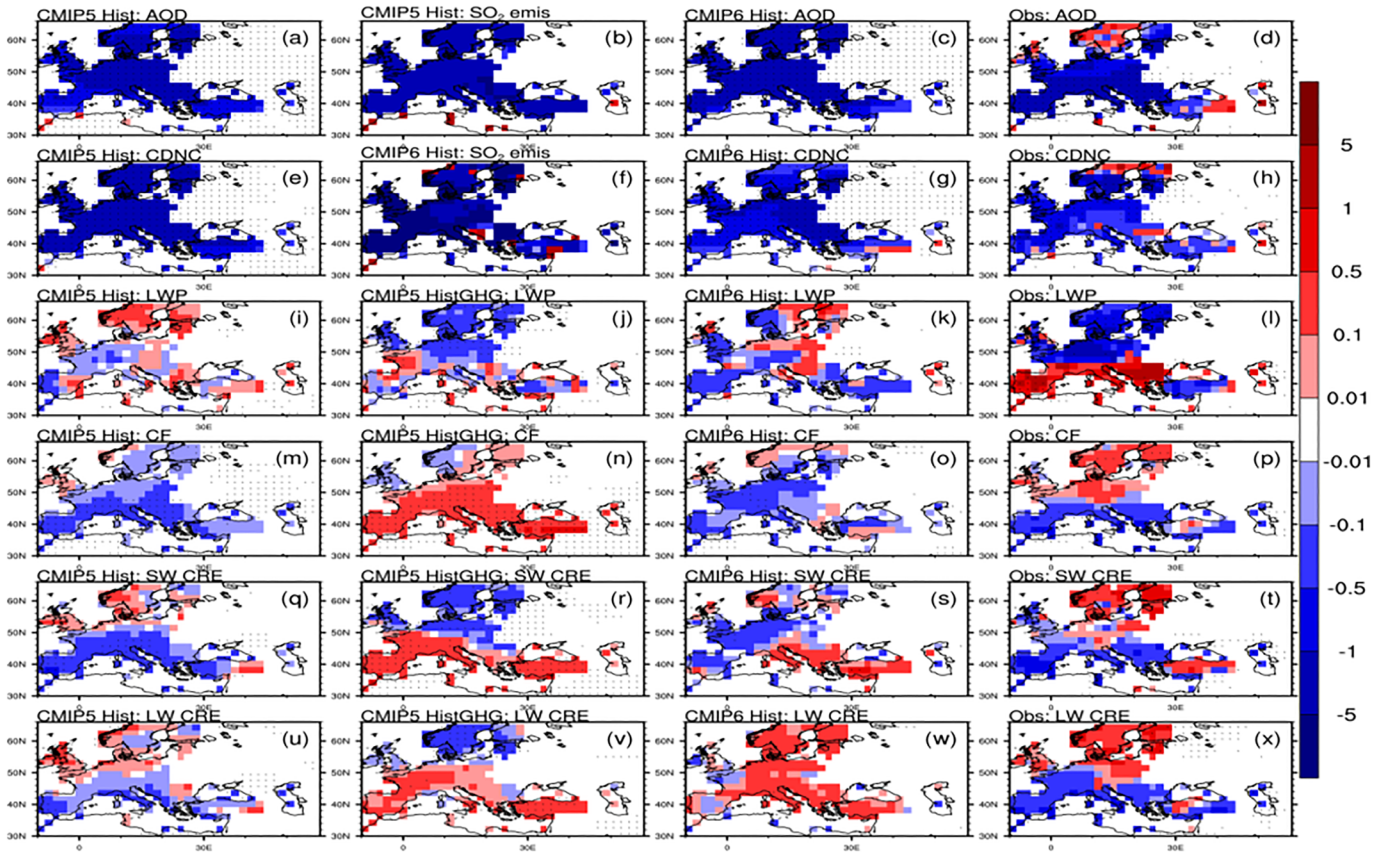

Figure 1. Linear trends between 2001 and 2017 for the Europe (EUR) region (% year^{-1} for AOD (a, c, and d), CDNC (e, g, and h), LWP (i–l), CF (m–p), SW CRE (q–t), and LW CRE (u–x) for multimodel mean (left column) CMIP5 historical run, (second column) CMIP5 historicalGHG, (third column) CMIP6 historical run, and (right column) satellite observations (MODIS in d, h, l, and p and CERES in t and x). CMIP5 and CMIP6 SO_2 emission trends are given in panels (b) and (f), respectively. Black dots indicate points where the trend is significant at the 95% confidence level.

AOD trends over China are challenging to simulate and interpret due to the trend reversal within the analyzed period. Anthropogenic SO_2 emissions were increasing until about 2005, approximately plateauing until 2010 and decreasing strongly since then (Figure S2). For China, trends are thus shown in two periods: first increasing (2001–2005, Figure S4) and second decreasing (2006–2017, Figure 4) periods. In the satellite retrievals, the net effect for the period examined here is a decrease for much of the region. The CMIP5 models completely failed to match this sign, they show increases over the entire country in both periods, of substantial magnitude especially in the eastern part of China. CMIP6 models, however, do show—as the observations—decreases since 2006 for most of the region, and increases in western parts of China (Figures 4c and 4d). The spatial distribution of increases trend is inconsistent with the one derived from the MODIS data. The results indicate that updated anthropogenic aerosol emission inventories improve the simulations in CMIP6 compared to CMIP5 (Figures 4f and S2). Previous studies reported (Zheng et al., 2018) the SO_2 emission trend reversal year (around 2005 to 2010) is well represented in CMIP6 emission inventories (Figure S2).

3.1.2. CDNC

In the EUR region, the satellite retrievals show mostly decreasing CDNC, consistent with the decreases in AOD. Both CMIP5 and CMIP6 models simulate the decreasing CDNC trend over the entire continent (Figures 1e–1h). The magnitude is too large for CMIP5, and this improves for CMIP6, although the data suggest somewhat weaker trends than even CMIP6.

For NAM, CMIP6 models simulate trends broadly consistent with the observed ones (increasing trend over western NAM and decreasing trend over eastern NAM), while CMIP5 models only simulate the decreasing trend over eastern NAM (Figures 2e–2h). It is interesting to note that the sign of the CDNC trend in the models mostly is consistent with the AOD trends. In the satellite retrievals, however, the widespread increase

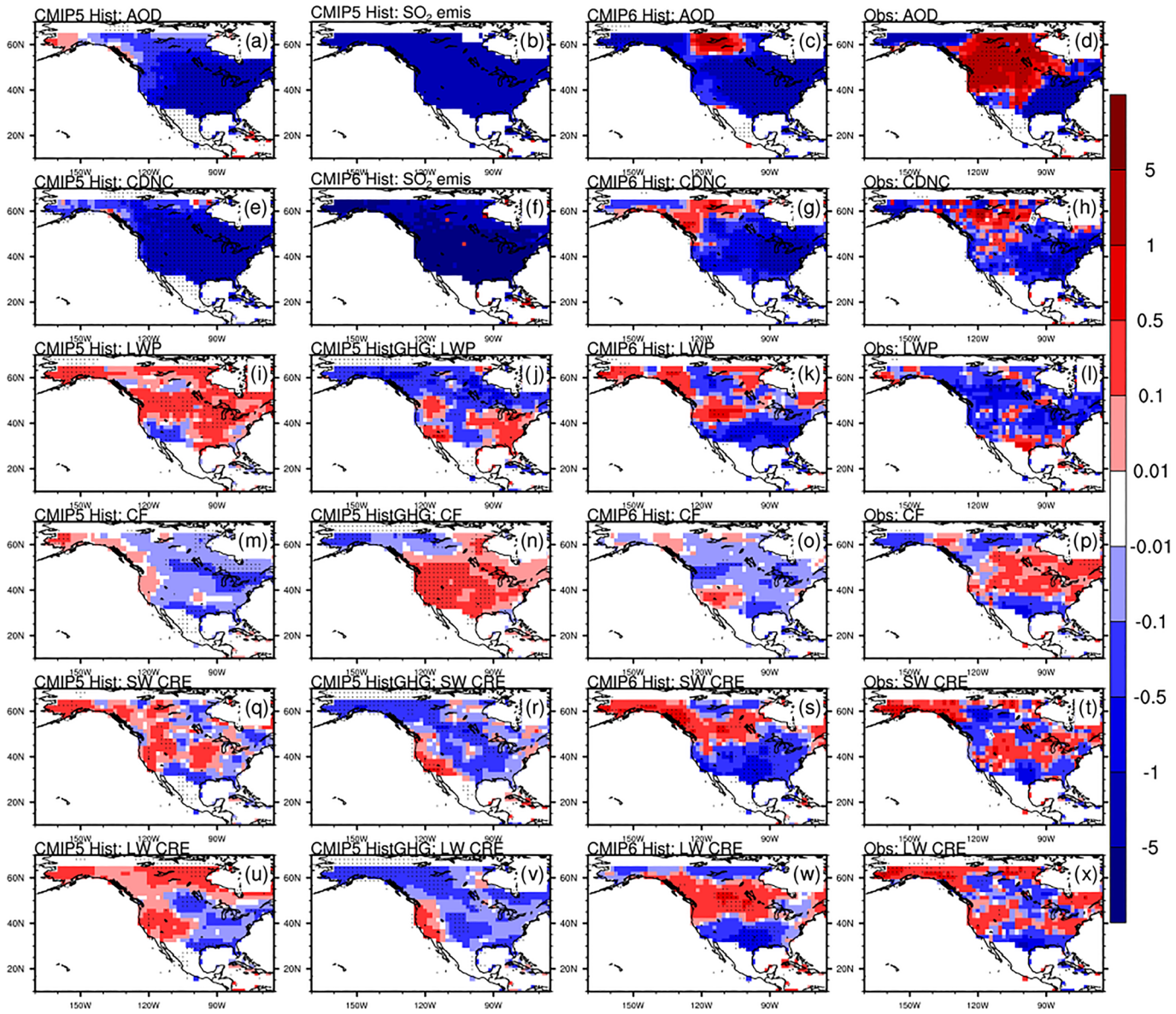

Figure 2. Same as Figure 1, but for the North American (NAM) region.

in AOD over much of the northwestern NAM is not consistent with the much more mixed result for CDNC: Only in a small portion of the northwest NAM, CDNC increases, whereas it decreases in the data over regions where the CMIP6 models also show a decrease.

Over India, the MODIS data suggest an increase over most of the subcontinent, but the signal is not regionally consistent: There are some parts of the region where CDNC in the satellite data shows a decrease. The models, in turn, both for CMIP5 and CMIP6, show increases consistent with the AOD increases.

Over China, the observation data suggest a widespread increase in CDNC in western, except for declines in the eastern part of the country. This latter decline is consistent with the AOD signal, but there are large areas in the center of the country where AOD shows declines, while CDNC shows increases. In the models, in contrast, the AOD and CDNC are largely of the same sign, as expected, and mostly show an increase. On average, CMIP6 results for CDNC are broadly consistent with the satellite results; whereas unlike the observations, CMIP5 show consistent increases.

In general, the CMIP6 ensemble shows improved model-simulated CNDC trends, compared to the satellite-derived trends, for EUR, NAM, India, and China regions. For both, models and—mostly

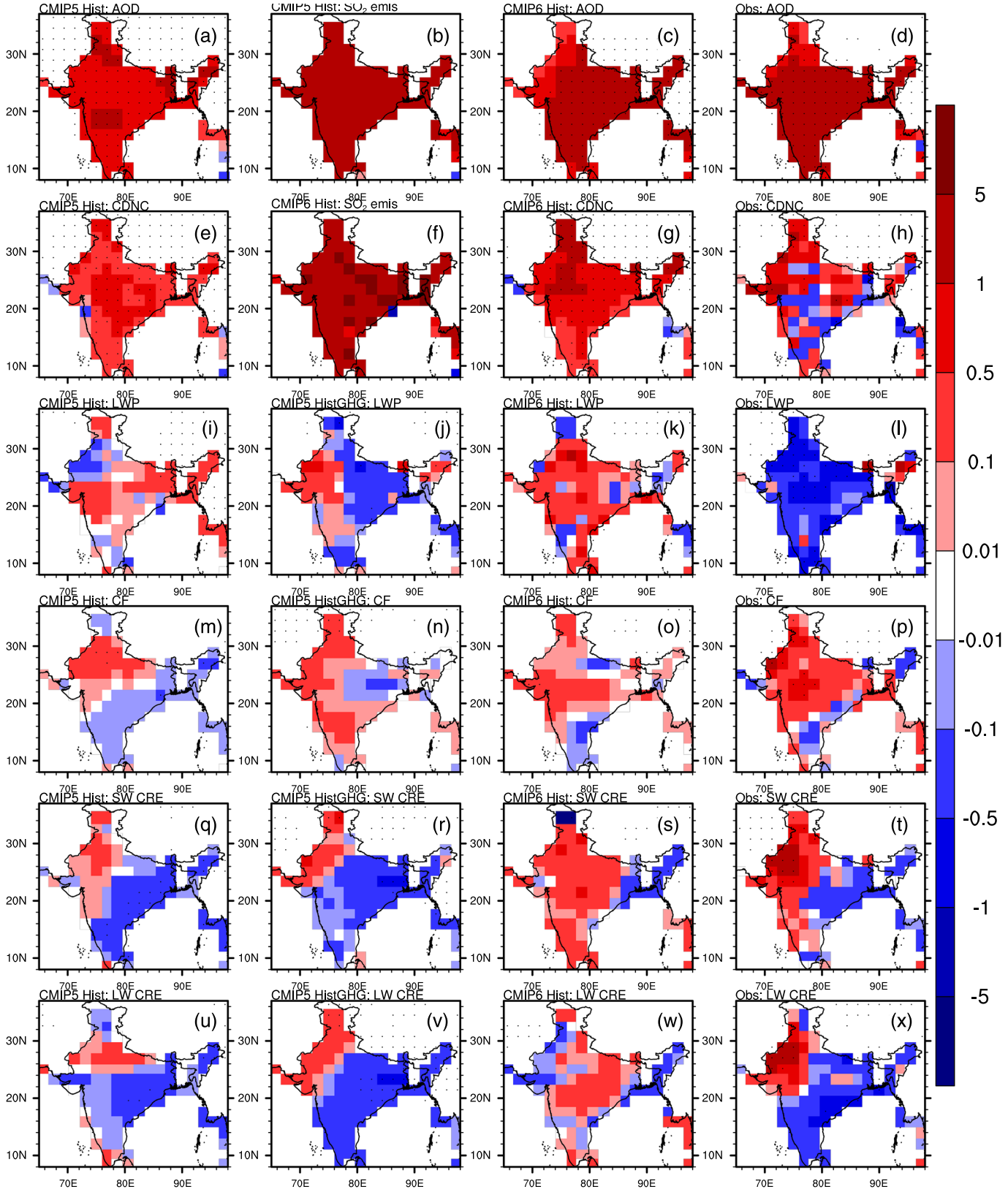

Figure 3. Same as Figure 1, but for India region.

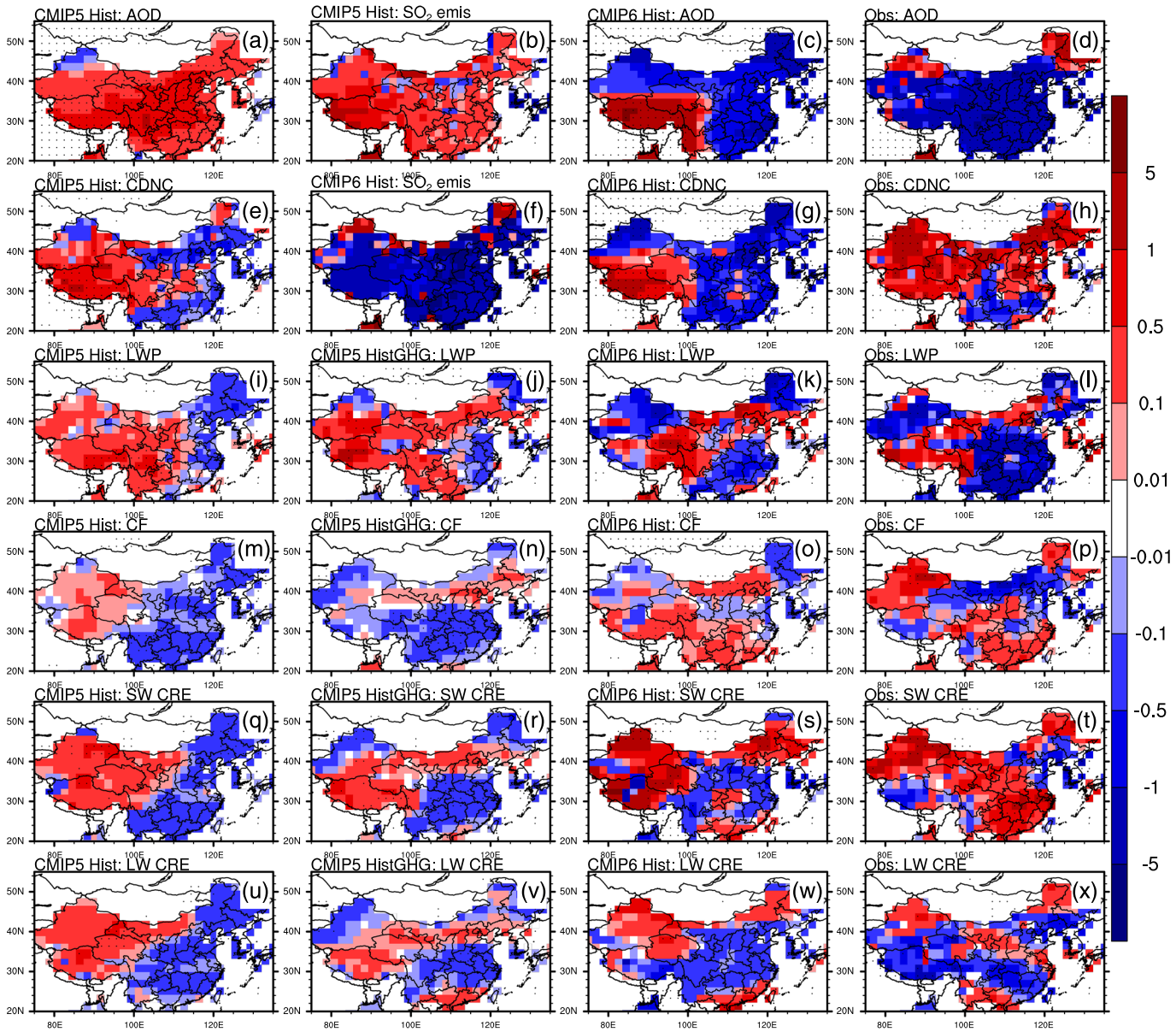

Figure 4. Same as Figure 1, but for the period of aerosol emission decreases from 2006 to 2017 over the China region.

also—satellite data, the signs of trends in CDNC are generally consistent with the AOD trends: where AOD increases, CDNC also increases, and decreases are consistent, too. This result is important since it highlights once again, but from a different perspective, the fact that there is a clear Twomey effect, or responses of CDNC to aerosol changes (Bellouin et al., 2019; Qian, Boucher, et al., 2009).

3.1.3. LWP And CF

Trends in LWP and CF are influenced by global warming (Norris et al., 2016) and also by aerosol emission trends. The expectation, based on model simulations, is that CF would decrease, and LWP increase, with warming (Zelinka et al., 2012). In contrast to this expectation, in the regions analyzed in Figures 1l to 4l, LWP from the satellite retrievals shows mostly decreasing trends, except for southern EUR, western, and mostly southwestern parts of China, and parts of NAM, especially in the south of this region, too.

The relation of LWP trends to the AOD trends is unclear: Over most of NAM, LWP decreases despite the differences between east and west in AOD trends (Figure 2l). Over India, however, there is a decrease in LWP along with the increase in AOD (Figure 3l). In turn, LWP shows strong decreases over eastern China, where AOD and CDNC decrease. The fact that two different LWP responses are possible was also discussed

in the context of statistical analysis of satellite data (Gryspeerdt et al., 2019). The model-simulated trends in LWP for either the CMIP5 or CMIP6 ensembles are in pattern, magnitude, and often even sign inconsistent with the results from the data. In order to disentangle the impact of the different forcing agents, the "historicalGHG" runs (CMIP5) are shown. These only consider the forcing by the greenhouse gases. In all four regions, this signal seems more consistent with the pattern shown by the satellite data than the "historical" simulations that include all forcings (also the aerosols). However, the signals in LWP are not the expected uniform increase in response to the warming but show also decreases, indicative of the LWP response to circulation changes.

It was highlighted in several studies that GCMs may tend to treat the response of LWP to aerosols incorrectly, by simulating an overly large positive response of LWP to additional aerosol (e.g., Malavelle et al., 2017;Michibata et al., 2016; Zhou & Penner, 2017). However, there is not a consistent correlation in LWP and CDNC signals in the models either; nevertheless, the combination of greenhouse gas and circulation effects with a possibly wrong LWP response may lead to this result of LWP trends that are inconsistent with the data.

The observed CF trends show results that are almost the inverse of the LWP trends in all four regions (Figure 1 to 4p). This is surprising given that often LWP and CF are positively correlated in the present-day climate. It is, in turn, expected from the GCM suggestions for the response to global warming (Zelinka et al., 2012). It is also consistent with global satellite analysis for the response to aerosols that overall is a slight decrease in LWP and increase in CF with increasing aerosol (Gryspeerdt et al., 2016; 2019). However, AOD and CF trends are not consistent across regions: Over India (Figures 3d and 3p), increases in AOD coincide with increases in CF, whereas over EUR, NAM, and China, the same sign in trends is only found for parts of the regions (southern part in EUR, northwestern part in NAM and western part of China). The models, in turn, simulate consistently decreasing trends in CF over EUR and NAM, but more mixed patterns over India and China (Figure 1 to 4 (m–o)). In response to only the greenhouse gases, CMIP5 models show the opposite trend in CF compared to the all-forcing runs, hinting at a role of the aerosols for the decrease in CF that is consistent with the decreasing CDNC trends in the EUR and NAM regions in the models.

3.1.4. CREs

The discussions are particularly relevant when discussing now the CRE changes. The patterns of trends in SW CRE in models ("historical" run) and satellite data match surprisingly well for the CMIP5 models, down to the subregional level (e.g., east-west split in trend sign over India, north-south split over EUR, middle vs. rest over NAM, border vs. rest over China; Figures 1- 4q-t). Similarly, LW CRE trends in "historical" model runs for the CMIP5 ensemble and satellite data agree well over EUR, NAM and central and south India regions (Figures 1- 4u-x). For EUR and NAM, the greenhouse-gas-only simulations in CMIP5, in turn, disagree with the patterns in the satellite data-derived trends, suggesting that the aerosol forcing plays an important role. The CRE changes are driven by the combination of CF and LWP changes. Over EUR and NAM, incorrect (compared to the satellite-derived trends) patterns in both LWP and CF trends compensate to yield a much more consistent pattern in CRE changes. Compensating errors in trends of LWP (overestimated by 5–10%) and CF (underestimated by 5–15%) lead to consistent CRE trends in CMIP5 models over EUR and NAM regions. This result is less striking but still evident also in the CMIP6 model ensemble. Over India, CMIP5 models show, despite the incorrect trend in LWP, a pattern in CRE that is consistent with the data, thanks to an overly strong CF reduction that, however, is not correlated to the CDNC signal. CMIP6 models do not show the southwest-northeast gradient in CRE trends. Over China, it is difficult to interpret the observational result: solar and terrestrial CRE show uncommon anticorrelated patterns of trends. The models, in turn, have consistent patterns between solar and terrestrial CRE.

4. Conclusion

The aim of the present study was to exploit the increasing length of the satellite record for aerosol and cloud properties, and the radiation budget, to investigate trends in AOD, CDNC, LWP, CF and solar and terrestrial CRE over four regions (EUR, NAM, India and China) that witnessed strong trends in anthropogenic aerosol emissions in the past 20 years along with global warming. Clouds And The Earth's Radiant Energy System (CERES) and MODIS satellite observations were used along with output from transient climate model simulations submitted to the CMIP5 and CMIP6 archives.

Comparisons revealed that model-simulated AOD and CDNC trends match well the satellite observations in EUR, eastern NAM, Northern China, and India, while model biases are visible in western NAM and southern China. In several subregions, CMIP6 AOD trends are more consistent with the satellite data than CMIP5, pointing to improvements in the aerosol emission data. The LWP trends do not clearly follow AOD trends in either models or satellite data. The models tend to simulate CF trends consistent with the AOD and CDNC trends, but this is not evident in the satellite data. Trends in CRE in the models match those in the satellite retrievals in some regions surprisingly well, but this result is due to compensating errors in the patterns of CF and LWP changes.

Acknowledgments
We thank two anonymous reviewers for their insightful and constructive comments that have led to several improvements. The climate modeling community, PCMDI, and the World Climate Data Centre, Hamburg, are acknowledged for providing the climate model results (https://esgf-node.llnl.gov/search/cmip6/). This research was funded by the Deutsche Forschungsgemeinschaft (DFG; German Research Foundation) project under Grant Agreement 637230; J. Q. also acknowledges funding by the European Union via its Horizon 2020 projects CONSTRAIN (GA 820829) and FORCeS (GA 821205).The MODIS Daily L3 Global 1 Deg. data sets were acquired from the Level-1 and Atmosphere Archive and Distribution System (LAADS) Distributed Active Archive Center (DAAC), located in the Goddard Space Flight Center in Greenbelt, Maryland (https://ladsweb.modaps.eosdis.nasa.gov/archive/allData/61/MOD08_D3/). The CERES EBAF Ed4.0 data set was obtained from the NASA Langley Research Center Atmospheric Science Data Center (https://ceres-tool.larc.nasa.gov/ord-tool/jsp/EBAF4Selection.jsp). The NCAR Command Language (NCL) has been used for data analysis and plotting.

References

Aas, W., Mortier, A., Bowersox, V., Cherian, R., Faluvegi, G., Fagerli, H., et al. (2019). Global and regional trends of atmospheric sulfur. *Scientific Reports*, *9*(1), 953. https://doi.org/10.1038/s41598-018-37304-0

Ackerman, A. S., Kirkpatrick, M. P., Stevens, D. E., & Toon, O. B. (2004). The impact of humidity above stratiform clouds on indirect aerosol climate forcing. *Nature*, *432*, 1014–1017. https://doi.org/10.1038/nature03174

Albrecht, B. A. (1989). Aerosols, cloud microphysics, and fractional cloudiness. *Science*, *245*(4923), 1227–1230. https://doi.org/10.1126/science.245.4923.1227

Arora, V. K., Scinocca, J. F., Boer, G. J., Christian, J. R., Denman, K. L., Flato, G. M., et al. (2011). Carbon emission limits required to satisfy future representative concentration pathways of greenhouse gases. *Geophysical Research Letters*, *38*, L05805. https://doi.org/10.1029/2010GL046270

Bellouin, N., Quaas, J., Gryspeerdt, E., Kinne, S., Stier, P., Watson-Parris, D., et al. (2019). Bounding global aerosol radiative forcing of climate change. *Reviews of Geophysics*, *58*, e2019RG000660. https://doi.org/10.1029/2019RG000660

Benas, N., Meirink, J. F., Karlsson, K.-G., Stengel, M., & Stammes, P. (2020). Satellite observations of aerosols and clouds over southern china from 2006 to 2015: Analysis of changes and possible interaction mechanisms. *Atmospheric Chemistry and Physics*, *20*(1), 457–474. https://doi.org/10.5194/acp-20-457-2020

Bennartz, R., Fan, J., Rausch, J., Leung, L. R., & Heidinger, A. K. (2011). Pollution from China increases cloud droplet number, suppresses rain over the East China Sea. *Geophysical Research Letters*, *38*, L09704. https://doi.org/10.1029/2011GL047235

Bentsen, M., Bethke, I., Debernard, J. B., Iversen, T., Kirkevåg, A., Seland, Ø., et al. (2013). The Norwegian Earth System Model, NorESM1-M—Part 1: Description and basic evaluation of the physical climate. *Geoscientific Model Development*, *6*(3), 687–720. https://doi.org/10.5194/gmd-6-687-2013

Boucher, O., Denvil, S., Caubel, A., & Foujols, M. A. (2018). *IPSL IPSL-CM6A-LR model output prepared for CMIP6 CMIP*. Paris, France: Earth System Grid Federation. https://doi.org/10.22033/ESGF/CMIP6.1534

Boucher, O., Randall, D., Artaxo, P., Bretherton, C., Feingold, G., Forster, P., et al. (2013). Clouds and aerosols [Book Section]. In T. Stocker (Ed.), *Climate change 2013: The physical science basis. Contribution of working group I to the fifth assessment report of the intergovernmental panel on climate change* pp. 571–658). Cambridge, United Kingdom and New York, NY, USA: Cambridge University Press. https://doi.org/10.1017/CBO9781107415324.016

Cherian, R., Quaas, J., Salzmann, M., & Wild, M. (2014). Pollution trends over europe constrain global aerosol forcing as simulated by climate models. *Geophysical Research Letters*, *41*, 2176–2181. https://doi.org/10.1002/2013GL058715

Chung, E.-S., & Soden, B. J. (2017). Hemispheric climate shifts driven by anthropogenic aerosol-cloud interactions. *Nature Geoscience*, *10*, 566–571. https://doi.org/10.1038/ngeo2988

Dolinar, E. K., Dong, X., Xi, B., Jiang, J. H., & Su, H. (2015). Evaluation of CMIP5 simulated clouds and TOA radiation budgets using NASA satellite observations. *Climate Dynamics*, *44*, 2229–2247. https://doi.org/10.1007/s00382-014-2158-9

Dong, X., & Mace, G. . (2003). Arctic stratus cloud properties and radiative forcing derived from ground-based data collected at Barrow, Alaska. *Journal of Climate*, *16*, 445–461. https://doi.org/10.1175/1520-0442(2003)016<0445:ASCPAR>2.0.CO;2

Donner, L. J., Wyman, B. L., Hemler, R. S., Horowitz, L. W., Ming, Y., Zhao, M., et al. (2011). The dynamical core, physical parameterizations, and basic simulation characteristics of the atmospheric component AM3 of the GFDL Global Coupled Model CM3. *Journal of Climate*, *24*(13), 3484–3519. https://doi.org/10.1175/2011JCLI3955.1

Dufresne, J.-L., Foujols, M.-A., Denvil, S., Caubel, A., Marti, O., Aumont, O., et al. (2013). Climate change projections using the IPSL-CM5 Earth System Model: From CMIP3 to CMIP5. *Climate Dynamics*, *40*(9), 2123–2165. https://doi.org/10.1007/s00382-012-1636-1

Ekman, A. M. L. (2014). Do sophisticated parameterizations of aerosol-cloud interactions in CMIP5 models improve the representation of recent observed temperature trends? *Journal of Geophysical Research: Atmospheres*, *119*, 817–832. https://doi.org/10.1002/2013JD020511

Eyring, V., Bony, S., Meehl, G. A., Senior, C. A., Stevens, B., Stouffer, R. J., & Taylor, K. E. (2016). Overview of the Coupled Model Intercomparison Project phase 6 (CMIP6) experimental design and organization. *Geoscientific Model Development*, *9*(5), 1937–1958. https://doi.org/10.5194/gmd-9-1937-2016

Fan, T., Zhao, C., Dong, X., Liu, X., Yang, X., Zhang, F., et al. (2018). Quantify contribution of aerosol errors to cloud fraction biases in CMIP5 atmospheric model intercomparison project simulations. *International Journal of Climatology*, *38*, 3140–3156. https://doi.org/10.1002/joc.5490

Flato, G., Marotzke, J., Abiodun, B., Braconnot, P., Chou, S., Collins, W., et al. (2013). Evaluation of climate models [Book Section]. In T. Stocker (Ed.), *Climate change 2013: The physical science basis. contribution of working group I to the fifth assessment report of the intergovernmental panel on climate change* (pp. 741–866). Cambridge, United Kingdom and New York, NY, USA: Cambridge University Press. https://doi.org/10.1017/CBO9781107415324.020

Geiss, A., & Marchand, R. (2019). Cloud responses to climate variability over the extratropical oceans as observed by MISR and MODIS. *Atmospheric Chemistry and Physics*, *19*(11), 7547–7565. https://doi.org/10.5194/acp-19-7547-2019

Gidden, M. J., Riahi, K., Smith, S. J., Fujimori, S., Luderer, G., Kriegler, E., et al. (2019). Global emissions pathways under different socioeconomic scenarios for use in CMIP6: A dataset of harmonized emissions trajectories through the end of the century. *Geoscientific Model Development*, *12*(4), 1443–1475. https://doi.org/10.5194/gmd-12-1443-2019

Gryspeerdt, E., Goren, T., Sourdeval, O., Quaas, J., Mülmenstädt, J., Dipu, S., et al. (2019). Constraining the aerosol influence on cloud liquid water path. *Atmospheric Chemistry and Physics*, *19*(8), 5331–5347. https://doi.org/10.5194/acp-19-5331-2019

Gryspeerdt, E., Quaas, J., & Bellouin, N. (2016). Constraining the aerosol influence on cloud fraction. *Journal of Geophysical Research: Atmospheres*, *121*(7), 3566–3583. https://doi.org/10.1002/2015JD023744

Hajima, T., Watanabe, M., Yamamoto, A., Tatebe, H., Noguchi, M. A., Abe, M., et al. (2019). Description of the MIROC-ES2L Earth System Model and evaluation of its climate-biogeochemical processes and feedbacks. *Geoscientific Model Development Discussions*, *2019*, 1–73. https://doi.org/10.5194/gmd-2019-275

Hasekamp, O. P., Edward, G., & Johannes, Q. (2019). Analysis of polarimetric satellite measurements suggests stronger cooling due to aerosol-cloud interactions. *Nature Communications. 10*, 5405. https://doi.org/10.1038/s41467-019-13372-2

Held, I. M., Guo, H., Adcroft, A., Dunne, J. P., Horowitz, L. W., Krasting, J., et al. (2019). Structure and performance of GFDL's CM4.0 climate model. *Journal of Advances in Modeling Earth Systems*, *11*, 3691–3727. https://doi.org/10.1029/2019MS001829

Hoesly, R. M., Smith, S. J., Feng, L., Klimont, Z., Janssens-Maenhout, G., Pitkanen, T., et al. (2018). Historical (1750–2014) anthropogenic emissions of reactive gases and aerosols from the Community Emissions Data System (CEDS). *Geoscientific Model Development*, *11*(1), 369–408. https://doi.org/10.5194/gmd-11-369-2018

Jiang, J. H., Su, H., Zhai, C., Perun, V. S., Genio, A. D., Nazarenko, L. S., et al. (2012). Evaluation of cloud and water vapor simulations in CMIP5 climate models using NASA "A-Train" satellite observations. *Journal of Geophysical Research*, *117*, D14105. https://doi.org/10.1029/2011JD017237

Jones, C. D., Hughes, J. K., Bellouin, N., Hardiman, S. C., Jones, G. S., Knight, J., et al. (2011). The HadGEM2-ES implementation of CMIP5 centennial simulations. *Geoscientific Model Development*, *4*(3), 543–570. https://doi.org/10.5194/gmd-4-543-2011

Jongeward, A. R., Li, Z., He, H., & Xiong, X. (2016). Natural and anthropogenic aerosol trends from satellite and surface observations and model simulations over the North Atlantic Ocean from 2002 to 2012. *Journal of the Atmospheric Sciences*, *4469–4485*(11). https://doi.org/10.1175/JAS-D-15-0308.1

Kim, D., Sobel, A. H., Del Genio, A. D., Chen, Y., Camargo, S. J., Yao, M.-S., et al. (2012). The tropical subseasonal variability simulated in the NASA GISS general circulation model. *Journal of Climate*, *25*(13), 4641–4659. https://doi.org/10.1175/JCLI-D-11-00447.1

Klein, S. A., & Hall, A. (2015). Emergent constraints for cloud feedbacks. *Current Climate Change Reports*, *1*(4), 276–287. https://doi.org/10.1007/s40641-015-0027-1

Klein, S. A., Zhang, Y., Zelinka, M. D., Pincus, R., Boyle, J., & Gleckler, P. J. (2013). Are climate model simulations of clouds improving? An evaluation using the ISCCP simulator. *Journal of Geophysical Research: Atmospheres*, *118*, 1329–1342. https://doi.org/10.1002/jgrd.50141

Klimont, Z., Smith, S. J., & Cofala, J. (2013). The last decade of global anthropogenic sulfur dioxide: 2000-2011 emissions. *Environmental Research Letters*, *8*(1), 014,003.

Krüger, O., & Graßl, H. (2002). The indirect aerosol effect over europe. *Geophysical Research Letters*, *29*(19), 31–1-31-4. https://doi.org/10.1029/2001GL014081

Lauer, A., & Hamilton, K. (2013). Simulating clouds with global climate models: A comparison on CMIP5 results with CMIP3 and satellite data. *Journal of Climate*, *26*, 3823–3845. https://doi.org/10.1175/JCLI-D-12-00451.1

Levy, R. C., Mattoo, S., Munchak, L. A., Remer, L. A., Sayer, A. M., Patadia, F., & Hsu, N. C. (2013). The collection 6 MODIS aerosol products overland and ocean. *Atmospheric Measurement Techniques*, *6*, 2989–3034.

Loeb, N. G., Wielicki, B. A., Su, W., Loukachine, K., Sun, W., Wong, T., et al. (2007). Multi-instrument comparison of top-of-atmosphere reflected solar radiation. *Journal of Climate*, *20*(3), 575–591. https://doi.org/10.1175/JCLI4018.1

Malavelle, F. F., Haywood, J. M., Jones, A., Gettelman, A., Clarisse, L., Bauduin, S., et al. (2017). Strong constraints on aerosol-cloud interactions from volcanic eruptions. *Nature*, *546*, 485–491. https://doi.org/10.1038/nature22974

Manaster, A., O'Dell, C. W., & Elsaesser, G. (2017). Evaluation of cloud liquid water path trends using a multidecadal record of passive microwave observations. *Journal of Climate*, *30*(15), 5871–5884. https://doi.org/10.1175/JCLI-D-16-0399.1

Michibata, T., Suzuki, K., Sato, Y., & Takemura, T. (2016). The source of discrepancies in aerosol–cloud–precipitation interactions between GCM and A-train retrievals. *Atmospheric Chemistry and Physics*, *16*(23), 15,413–15,424. https://doi.org/10.5194/acp-16-15413-2016

Myhre, G., Aas, W., Cherian, R., Collins, W., Faluvegl, G., Flanner, M., et al. (2017). Multi-model simulations of aerosol and ozone radiative forcing due to anthropogenic emission changes during the period 1990-2015. *Atmospheric Chemistry and Physics*, *17*, 2709–2720. https://doi.org/10.5194/acp-17-2709-2017

Myhre, G., Shindell, D., Br'eon, F.-M., Collins, W., Fuglestvedt, J., Huang, J., et al. (2013). Anthropogenic and natural radiative forcing [Book Section], *Climate change 2013: The physical science basis. Contribution of working group I to the fifth assessment report of the intergovernmental panel on climate change* pp. 659–740). Cambridge, United Kingdom and New York, NY, USA: Cambridge University Press. https://doi.org/10.1017/CBO9781107415324.018

Norris, J. R., Allen, R. J., Evan, A. T., Zelinka, M. D., O'Dell, C. W., & Klein, S. A. (2016). Evidence for climate change in the satellite cloud record. *Nature*, *536*, 72–75. https://doi.org/10.1038/nature18273

Norris, J. R., & Wild, M. (2007). Trends in aerosol radiative effects over Europe inferred from observed cloud cover, solar "dimming," and solar "brightening". *Journal of Geophysical Research*, *112*, D08214. https://doi.org/10.1029/2006JD007794

O'Neill, B. C., Tebaldi, C., van Vuuren, D. P., Eyring, V., Friedlingstein, P., Hurtt, G., et al. (2016). The scenario model intercomparison project (ScenarioMIP) for CMIP6. *Geoscientific Model Development*, *9*(9), 3461–3482. https://doi.org/10.5194/gmd-9-3461-2016

Platnick, S., Meyer, K. G., King, M. D., Wind, G., Amarasinghe, N., Marchant, B., et al. (2017). The modis cloud optical and microphysical products: Collection 6 updates and examples from Terra and Aqua. *IEEE Transactions on Geoscience and Remote Sensing*, *55*(1), 502–525. https://doi.org/10.1109/TGRS.2016.2610522

Qian, Y., Gong, D., Fan, J., Leung, L. R., Bennartz, R., Chen, D., & Wang, W. (2009). Heavy pollution suppresses light rain in china: Observations and modeling. *Journal of Geophysical Research*, *114*, D00K02. https://doi.org/10.1029/2008JD011575

Quaas, J., Boucher, O., Jones, A., Weedon, G. P., Kieser, J., & Joos, H. (2009). Exploiting the weekly cycle as observed over europe to analyse aerosol indirect effects in two climate models. *Atmospheric Chemistry and Physics*, *9*(21), 8493–8501. https://doi.org/10.5194/acp-9-8493-2009

Quaas, J., Boucher, O., & Lohmann, U. (2006). Constraining the total aerosol indirect effect in the LMDZ and ECHAM4 GCMs using modis satellite data. *Atmospheric Chemistry and Physics*, *6*(4), 947—955. https://doi.org/10.5194/acp-6-947-2006

Ramanathan, V. (1989). Cloud-radiative forcing and climate: Results from the Earth radiation budget experiment. *Science*, *243*, 57–63. https://doi.org/10.1126/science.243.4887.57

Roberts, M. (2017). MOHC HadGEM3-GC31-LL model output prepared for CMIP6 HighResMIP. *Earth System Grid Federation*. https://doi.org/10.22033/ESGF/CMIP6.1901

Smith, S. J., & Bond, T. C. (2014). Two hundred fifty years of aerosols and climate: The end of the age of aerosols. *Atmospheric Chemistry and Physics*, *14*, 537–549. https://doi.org/10.5194/acp-14-537-2014

Stanfield, R. E., Dong, X., Xi, B., Del Genio, A. D., Minnis, P., Doelling, D., & Loeb, N. (2015). Assessment of NASA GISS CMIP5 and Post-CMIP5 Simulated Clouds and TOA Radiation Budgets Using Satellite Observations. Part II: TOA Radiation Budget and CREs. *Journal of Climate*, *28*(5), 1842–1864. https://doi.org/10.1175/JCLI-D-14-00249.1

Stanfield, R. E., Dong, X., Xi, B., Kennedy, A., Del Genio, A. D., Minnis, P., & Jiang, J. H. (2014). Assessment of NASA GISS CMIP5 and post-CMIP5 simulated clouds and TOA radiation budgets using satellite observations: Part I: Cloud fraction and properties. *Journal of Climate*, *27*(11), 4189–4208. https://doi.org/10.1175/JCLI-D-13-00558.1

Stohl, A., Aamaas, B., Amann, M., Baker, L. H., Bellouin, N., Berntsen, T. K., et al. (2015). Evaluating the climate and air quality impacts of short-lived pollutants. *Atmospheric Chemistry and Physics*, *15*(18), 10,529–10,566. https://doi.org/10.5194/acp-15-10529-2015

Swart, N. C., Cole, J. N. S., Kharin, V. V., Lazare, M., Scinocca, J. F., Gillett, N. P., et al. (2019). The Canadian Earth System Model version 5 (CanESM5.0.3). *Geoscientific Model Development*, *12*(11), 4823–4873. https://doi.org/10.5194/gmd-12-4823-2019

Taylor, K. E., Stouffer, R. J., & Meehl, G. A. (2012). An overview of CMIP5 and the experiment design. *Bulletin of the American Meteorological Society*, *93*(4), 485–498. https://doi.org/10.1175/BAMS-D-11-00094.1

Toll, V., Christensen, M., Gassó, S., & Bellouin, N. (2017). Volcano and ship tracks indicate excessive aerosol-induced cloud water increases in a climate model. *Geophysical Research Letters*, *44*, 12,492–12,500. https://doi.org/10.1002/2017GL075280

Toll, V., Christensen, M., Quaas, J., & Bellouin, N. (2019). Weak average liquid-cloud-water response to anthropogenic aerosols. *Nature*, *572*, 51–55. https://doi.org/10.1038/s41586-019-1423-9

Twomey, S. (1974). Pollution and the planetary albedo. *Atmospheric Environment*, *8*(12), 1251–1256. https://doi.org/10.1016/0004-6981(74)90004-3

Wang, H., & Su, W. (2013). Evaluating and understanding top of the atmosphere cloud radiative effects in International Panel on Climate Change (IPCC) AR5 CMIP5 models using satellite observations. *Journal of Geophysical Research: Atmospheres*, *118*, 683–699. https://doi.org/10.1029/2012JD018619

Watanabe, M., Suzuki, T., O'ishi, R., Komuro, Y., Watanabe, S., Emori, S., et al. (2010). Improved climate simulation by MIROC5: Mean states, variability, and climate sensitivity. *Journal of Climate*, *23*(23), 6312–6335. https://doi.org/10.1175/2010JCLI3679.1

Wei, J., Peng, Y., Guo, J., & Sun, L. (2019). Performance of MODIS collection 6.1 level 3 aerosol products in spatial-temporal variations over land. *Atmospheric Environment*, *206*, 30–44. https://doi.org/10.1016/j.atmosenv.2019.03.001

Wei, J., Peng, Y., Mahmood, R., Sun, L., & Guo, J. (2019). Intercomparison in spatial distributions and temporal trends derived from multi-source satellite aerosol products. *Atmospheric Chemistry and Physics*, *19*(10), 7183–7207. https://doi.org/10.5194/acp-19-7183-2019

Wild, M., Gilgen, H., Roesch, A., Ohmura, A., Long, C. N., Dutton, E. G., et al. (2005). From dimming to brightening: Decadal changes in solar radiation at Earth's surface. *Science*, *308*(5723), 847–850. https://doi.org/10.1126/science.1103215

Yoon, J., Burrows, J. P., Vountas, M., von Hoyningen-Huene, W., Chang, D. Y., Richter, A., & Hilboll, A. (2014). Changes in atmospheric aerosol loading retrieved from space-based measurements during the past decade. *Atmospheric Chemistry and Physics*, *14*(13), 6881–6902. https://doi.org/10.5194/acp-14-6881-2014

Yu, H., Yang, Y., Wang, H., Tan, Q., Chin, M., Levy, R. C., et al. (2020). Interannual variability and trends of combustion aerosol and dust in major continental outflows revealed by modis retrievals and CAM5 simulations during 2003–2017. *Atmospheric Chemistry and Physics*, *20*(1), 139–161. https://doi.org/10.5194/acp-20-139-2020

Zelinka, M. D., Klein, S. A., & Hartmann, D. L. (2012). Computing and partitioning cloud feedbacks using cloud property histograms. Part II: Attribution to changes in cloud amount, altitude, and optical depth. *Journal of Climate*, *25*(11), 3736–3754. https://doi.org/10.1175/JCLI-D-11-00249.1

Zheng, B., Tong, D., Li, M., Liu, F., Hong, C., Geng, G., et al. (2018). Trends in China's anthropogenic emissions since 2010 as the consequence of clean air actions. *Atmospheric Chemistry and Physics*, *18*(19), 14,095–14,111. https://doi.org/10.5194/acp-18-14095-2018

Zhou, C., & Penner, J. E. (2017). Why do general circulation models overestimate the aerosol cloud lifetime effect? A case study comparing CAM5 and a CRM. *Atmospheric Chemistry and Physics*, *17*(1), 21–29. https://doi.org/10.5194/acp-17-21-2017